J. Biochem. **141,** 889–895 (2007)
doi:10.1093/jb/mvm095

Spatial Orientation of Mitochondrial Processing Peptidase and a Preprotein Revealed by Fluorescence Resonance Energy Transfer†

Tomonori G. Nishino[1], Ken Kitano[2], Katsuhiko Kojima[1], Tadashi Ogishima[1], Akio Ito[1] and Sakae Kitada[1,*]

[1]*Department of Chemistry, Faculty of Science, Kyushu University, Fukuoka 812-8581, Japan; and*
[2]*Structural Biology Laboratory, Nara Institute of Science and Technology, Takayama, Ikoma, Nara, Japan*

Received February 6, 2007; accepted April 2, 2007; published online April 10, 2007

Mitochondrial processing peptidase (MPP), which is composed of heterodimeric α-MPP and β-MPP subunits. It specifically recognizes mitochondrial preproteins and removes their basic N-terminal signal prepeptides. In order to elucidate the spatial orientation of the preproteins toward MPP, which has been missed by crystal structures of a yeast MPP including a synthetic prepeptide in its acidic proteolytic chamber, we analysed the fluorescence resonance energy transfer (FRET) between EGFP fused to a yeast aconitase presequence (preEGFP) and regiospecific 7-dietylamino-3-(4′-maleimidyl phenyl)-4-methyl coumarin (CPM)-labelled yeast MPPs. FRET efficiencies of 65 and 55% were observed between the EGFP chromophore and CPM-Ser^{84} and -Lys^{156} of β-MPP, respectively, leading to calculated distances between the molecules of 48 and 50 Å, respectively. Considering the FRET results and the structural validity based on the crystal structure of the MPP-presequence complex, a plausible model of preEGFP associated with MPP was constructed *in silico*. The modelled structure indicated that amino acid residues on the C-terminal side of the cleavage site in the preprotein were orientated tail out from the large cavity of MPP and interacted with the glycine-rich loop of α-MPP. Thus, MPP orientates preproteins at the specific cleft between the catalytic domain and the flexible glycine-rich loop which seems to pinch the extended polypeptide.

Key words: FRET, GFP, mitochondria, processing, protease.

Abbreviations: ACON, aconitase; COX IV, cytochrome *c* oxidase subunit IV; CPM, 7-dietylamino-3-(4′-maleimidyl phenyl)-4-methyl coumarin; EGFP, enhanced green fluorescent protein; FRET, fluorescence resonance energy transfer; MDH, malate dehydrogenase; MPP, mitochondrial processing peptidase; preEGFP, presequence-fused EGFP; TIM, translocase on the inner mitochondrial membrane; TOM, translocase on the outer mitochondrial membrane.

Mitochondrial preproteins are synthesized in cytosolic ribosomes and imported into the matrix through a translocase machinery consisting of a translocase on the outer mitochondrial membrane (TOM[1]) and a translocase on the inner mitochondrial membrane (TIM) (*2–4*). After or during the transport, the N-terminal presequences of most preproteins are removed by mitochondrial processing peptidase (MPP) (*5*). MPP cleaves not only presequences but also sites between two polypeptide domains of polyproteins (*6*). This proteolytic processing is involved in the maturation of mitochondrial proteins, and the protease actions are therefore tightly regulated and specifically catalysed.

MPP is a heterodimeric zinc-metalloendopeptidase consisting of regulatory α-MPP and catalytic β-MPP subunits (*7*, *8*). It recognizes the basic presequences of various mitochondrial proteins, although the presequences show poor sequence homology. The mechanisms for how MPP recognizes these presequences and cleaves proteins at specific sites remain to be fully elucidated. Extensive studies have indicated that MPP associates with presequences though electrostatic interactions (*8*) and processes them at a general cleavage motif, -RX↓ΦΨΨ- (where X is any amino acid, Φ and Ψ indicate hydrophobic and hydrophilic amino acids, respectively and ↓ indicates the cleavage site) (*6, 9–13*).

Mutation analyses for MPPs have been reported and the target residues are usually acidic amino acids, since MPP recognizes basic sites in the presequences. The glutamate residues of yeast α-MPP contribute to the recognition of basic amino acids in longer presequences which are located at distal regions from the cleavage sites (*14–16*), while the Glu^{191} and Asp^{195} residues in rat β-MPP recognize the arginine residue at position −2 (P_2^2) from the preprotein cleavage site (*14–16*). Moreover, studies using fluorescent probes have revealed that MPP

†Following Schechter and Berger (*1*), the enzyme binding sites are denoted S_1, … S_2, …, S_i and S_1', S_2', …, S_i' away from the scissile peptide bond toward the N- and C-termini, respectively. The amino acid residues in the substrates are referred to as P_1, P_2, …, P_i and P_1', P_2', …, P_i' in accordance with the binding site.

*To whom correspondence should be addressed. Tel: +81-92-642-4182, Fax: +81-92-642-2607,
E-mail: s.kitscc@mbox.nc.kyushu-u.ac.jp

accommodates the substrate peptide into the putative cavity between α-MPP and β-MPP and that the peptide is extended in the cavity (*17–19*), while NMR analyses have indicated that the targeting signal is recognized at the level of the helical structure by the presequence receptor Tom20 (*17–19*).

The X-ray crystal structures of a yeast MPP complexed with synthesized presequence peptides of malate dehydrogenase (MDH) and cytochrome *c* oxidase subunit IV (COX IV) have been determined (*20*). MPP incorporated the presequences into the internal molecular cavity, possibly through a narrow cleft between the subunits. The structures also provided evidence of electrostatic interactions between MPP and the presequences, and indicated that the P_2–S_2 and $P'_1-S'_1$ interactions could provide the enzyme cleavage site specificity. However, P'_2 and P'_3 composed of hydrophilic amino acids with hydroxy groups in their side chains remain to be determined because the electron densities around the C-terminal regions of the substrate peptides were so low that structural analysis around P'_2 and P'_3 was unsuccessful. Therefore, the specific regions that interact with the P'_2 and P'_3 sites and the orientation of the mature polypeptides toward MPP remain unknown.

In the present study, we elucidated the C-terminal orientation from the cleavage site of the preprotein by investigating the fluorescence resonance energy transfer (FRET) between regiospecifically fluorescently labelled MPPs and an artificial green fluorescence preprotein (preEGFP). From the results of molecular modelling based on the distances calculated from the FRET analysis and the X-ray crystal structure of the MPP–prepeptide complex, we conclude that the polypeptide of the preprotein sticks out from the cavity through the cleft by the side of the active centre containing the zinc (II) ion of β-MPP and the glycine-rich loop region of α-MPP.

EXPERIMENTAL PROCEDURES

Purification of Regiospecifically Fluorescently Labelled MPP—Yeast *S. cerevisiae* β-MPP$^{E73Q/C252S/S84C}$, β-MPP$^{E73Q/C252S/K156C}$ and β-MPP$^{E73Q/C252S/N316C}$ were engineered by mutation of Ser^{84}, Lys^{156} and Asn^{316} of β-MPP$^{E73Q/C252S}$, containing a C-terminal hexahistidine (His_6) tag (*19*), to cysteine residues, respectively, using a QuickChange site-directed mutagenesis kit (Stratagene). The His_6-tagged yeast MPPs were expressed in *Escherichia coli* strain BL21-CodonPlus(DE3) (Stratagene) and purified with Hi-Trap chelating columns (GE Healthcare) as previously described (*17*, *19*). The purified β-MPPs were mixed with 0.1 mM 7-dietylamino-3-(4′-maleimidyl phenyl)-4-methyl coumarin (CPM; Molecular Probes) and rotated at 4°C for 2 h. To terminate the reaction, 1 M cysteine (pH 7.0) was added and the mixture was rotated at 4°C for a further 2 h. The free probes were removed with PD-10 desalting columns equilibrated with 20 mM HEPES–KOH (pH 7.5), 200 mM NaCl and 30% glycerol. The CPM-modified β-MPPs were diluted 1:10 with buffer Q [20 mM HEPES–KOH (pH 7.5) and 30% glycerol], and applied to a TOYOPEARL SuperQ-650 (Tosoh) column equilibrated with buffer Q containing 20 mM NaCl. After washing the column with the equilibration buffer, the labelled β-MPP was eluted with 100 mM NaCl. CPM-labelling efficiencies and protein purities were examined by SDS–PAGE followed by UV transillumination and Coomassie Brilliant Blue staining. The CPM-labelling efficiencies were calculated using a molar extinction coefficient of 33,000 ($M^{-1}\,cm^{-1}$) at 384 nm for CPM. Equal molar amounts of α-MPP and βMPP were mixed and the MPP complex was used for FRET measurements.

Preparation of preEGFP—A C-terminally His_6-tagged preEGFP was designed by adding the N-terminal sequence of aconitase (preACON; amino acids 1–20), containing the C-terminal five residues from the MPP cleavage site, to the N-terminus of EGFP. The EGFP gene was amplified by PCR from the pEGFP-C3 vector (Clontech) using 5′- and 3′-primers containing *Eco*R I and *Xho* I sites, respectively, and inserted into the *Eco*R I and *Xho* I sites of the pET-23d vector (Novagen). A DNA fragment including the presequence of preACON was amplified from *S. cerevisiae* genomic DNA by PCR using 5′- and 3′-primers containing *Nco* I and *Eco*R I sites, respectively. The DNA was digested and ligated into the *Nco* I and *Eco*R I sites of pET-23d, where the EGFP cDNA was inserted. The preEGFP protein was expressed in *E. coli* strain BL21-CodonPlus(DE3). The cells were extracted and loaded onto a Hi-Trap chelating column as described previously (*17*, *19*). The column was washed with 20 mM HEPES–KOH (pH 7.5), 100 mM NaCl and 30% glycerol containing 50 mM imidazole, and the preEGFP was eluted with the same buffer containing 100 mM imidazole. The fractions containing the fusion protein were desalted as described for the MPP preparation. The purity was analysed by SDS–PAGE followed by Coomassie Brilliant Blue staining, and the concentration was calculated using a molar extinction coefficient of 55,000 ($M^{-1}\,cm^{-1}$) at 489 nm for EGFP (*21*).

Fluorescence Measurements—The quantum yield of the donor (Φ_D) was given by Equation 1.

$$\Phi_D=\Phi_{st}(F_D A_{st})/F_{st}A_D) \quad (1)$$

The total fluorescence intensities of fluorescein dissolved in 0.1 N NaOH and CPM bound to the β-MPP mutants were measured in an F-4500 fluorescence spectrophotometer (Hitachi) as the standard (F_{st}) and donor (F_D) fluorescence intensities, respectively. The absorbances (A_{st} and A_D) at the excitation wavelengths of fluorescein and CPM bound to the β-MPP mutants, respectively, were measured in a UV-2500 PC spectrophotometer (Shimadzu). The quantum yield for fluorescein (Φ_{st}) was assumed to be 0.92 in 0.1 N NaOH. The spectral overlap (J) between the emission spectrum of CPM bound to the β-MPP mutants and the absorption spectrum of preEGFP was given by Equation 2.

$$J = \int F_D(\lambda)\varepsilon_A(\lambda)\lambda^4 d\lambda / \int F_D(\lambda)d\lambda \quad (2)$$

Here, λ means wavelength, and $F_D(\lambda)$ and $\varepsilon_A(\lambda)$ indicate the fluorescence intensity of CPM bound to the β-MPP mutants and the molar extinction coefficient of preEGFP, respectively, at the wavelength of λ λnm̃. FRET analysis

was performed as follows. The preEGFP was added at various concentrations ([S]; 0–0.4 μM) to buffer Q containing 0.1 μM CPM-labelled MPP. The CPM-labelled MPP was excited at 370 nm, a wavelength at which EGFP could be excited but its emission spectrum did not affect the fluorescence intensity at 465 nm where the peak of CPM exists. The fluorescence spectra were scanned from 400 to 600 nm and the fluorescence intensities at 465 nm (F) were recorded. A decrease in the fluorescence intensity (dF) was expressed by Equation 3, where F_0 means the fluorescence intensity in the absence of preEGFP.

$$dF = F_0 - F \quad (3)$$

The relationship between the concentration of preEGFP ([S]) and dF was given by Equation 4.

$$dF = F_{\max}[S]/(K_d + [S]) \quad (4)$$

To determine the maximal decrease in the fluorescence intensity ($dF_{\max}$) and the dissociation constant (K_d), a linear approximation was carried out using a Hanes–Woolf plot ([S]/dF versus [S]). In this plot, the slope and y-intercept provide $1/dF_{\max}$ and $K_d/dF_{\max}$, respectively. From the energy transfer efficiency ($E_T = dF_{\max}/F_0$), the distance (R) between the donor and acceptor was calculated according to the Förster theory as shown in Equation 5.

$$R = R_0(1/E_T - 1)^{1/6} \quad (5)$$

The Förster distance (R_0) indicates the distance at which half the energy emitted from the donor was transferred to the acceptor and is defined by Equation 6.

$$R_0^6 = 9000(\ln\ 10)J\kappa^2\Phi_D/128\pi^5 n^4 N_A \quad (6)$$

In Equation 6, κ^2, n and N_A are the orientation factor, reflective index of the solution and Avogadro's number, respectively, and are assumed to be 2/3, 1.4 and 6.02×10^{23}, respectively.

Structural Modelling of preEGFP Complexed with MPP—A structural model of the MPP–preEGFP complex was constructed *in silico*, based on the crystal structure of a yeast MPP complexed with the COX IV peptide (PDB ID: 1HR8) (*20*) and the structure of EGFP (PDB ID: 1JBZ) (*22*). The EGFP structure (residues 26–251, re-numbered due to the addition of the N-terminal preACON) was superimposed and oriented toward MPP using program O (*23*). A model of the eight linking residues (^{18}TVSEFVSK^{25}) was manually built using program O (*23*), followed by structural refinement (conjugate gradient minimization) using program CNS (*24*) with no experimental energy terms. The stereochemistry of the eight modelled residues was assessed by Procheck (*25*), which indicated that five residues were observed in the most favoured region and three residues were present in the additional allowed region of the Ramachandran plot.

RESULTS

Fluorescently Labelled MPP and Processing of preEGFP—For FRET analysis, a yeast recombinant MPP modified with CPM, which binds to the thiol group of cysteine residues, was used as a fluorescence donor, while the chromophore of preEGFP was employed as a fluorescence acceptor. At first, we adopted β-MPP$^{E73Q/C252S}$, a catalytically defective mutant subunit of MPP that retains a substrate-binding ability, in which βGlu^{73} was substituted to βGln^{73} and the sole βCys^{252} was mutated to βSer^{252} (*19*). To regiospecifically introduce CPM into yeast β-MPP, three adequate amino acid residues (Ser^{84}, Lys^{156} and Asn^{316}) in β-MPP were selected, and independently substituted to cysteines. These resides matched the criteria for fluorescence-labelling sites as follows: side chain facing the molecular surface, located along the cleft and irrelevant to the catalytic activity or structural stability (Fig. 1A). The cysteine-variants of the recombinant β-MPPs were purified and modified with CPM. Since the β-MPP mutant proteins were specifically labelled with CPM,

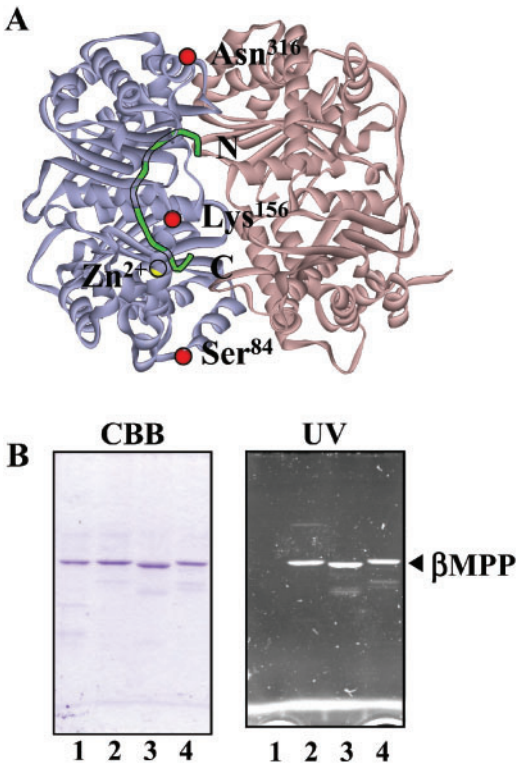

Fig 1. **Regiospecific fluorescence-labelling of MPP.** (A) Crystal structure of MPP complexed with the COX IV prepeptide (PDB ID: 1HR8) (*20*) displayed with ViewerLite 5.0 (Accelrys Inc.). The red and blue ribbons display α-MPP and β-MPP, respectively. The COX IV presequence peptide, which has a cleavage site for MPP between Thr^{17} and Leu^{18}, is shown as a green tube, and N and C indicate the N- and C-terminus of the peptide, respectively. The yellow ball and three red balls represent the Zn(II) ion at the active centre and the α-carbons of Ser^{84}, Lys^{156} and Asn^{316} in β-MPP, respectively. (B) CPM-labelling of cysteine variants of β-MPP. β-MPP^{E73Q}, β-MPP^{84CPM}, β-MPP^{156CPM} and β-MPP^{316CPM} (*lanes 1*, *2*, *3* and *4*, respectively) were separated by SDS–PAGE and stained with Coomassie Brilliant Blue (*left panel*). To examine the fluorescence of the labelled-β-MPPs, the gel shown in the left panel was detected by UV illumination using a cooled CCD camera system (Light-Capture; ATTO) (*right panel*).

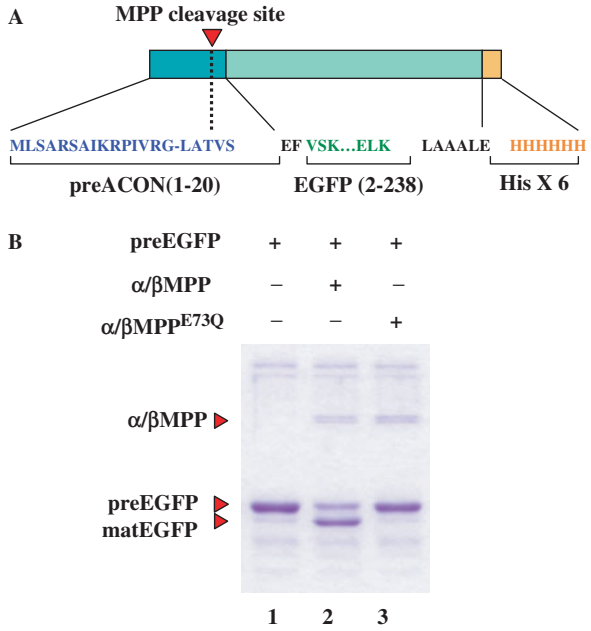

Fig 2. **Processing of preEGFP.** (A) Schematic diagram of the primary structure of preEGFP. The regions and sequences of the yeast preACON, EGFP and polyhistidine tag are indicated in blue, green and yellow, respectively. The MPP cleavage site is denoted by a dashed line and an arrowhead. (B) Processing of preEGFP by MPP. Purified preEGFP was mixed with α/β-MPP or α/β-MPP^{E73Q} and incubated at 30°C for 30 min. Next, the proteins were separated by SDS–PAGE and stained with Coomassie Brilliant Blue. Both wild-type α/β-MPP and the active site mutant (α/β-MPP^{E73Q}) are detected as doublets, indicating the presence of larger (α-MPP) and smaller (β-MPP) subunits. Note that a mature form of preEGFP (matEGFP) is only detected after incubation with wild-type MPP.

modifications could occur at the thiol-groups of the introduced sole cysteines (Fig. 1B). On the other hand, we also engineered and purified preEGFP, consisting of the N-terminal presequence of aconitase (Fig. 2A). The preEGFP was processed by wild-type MPP but not by the catalytically defective MPP mutant (α/β-MPP^{E73Q}) (Fig. 2B). Thus, MPP is able to recognize and cleave the artificial fusion protein.

FRET Analysis and Distance Calculation between CPM on MPP and the Chromophore in preEGFP—The fluorescence spectra of the CPM-labelled MPPs (MPP^{84CPM}, MPP^{156CPM} and MPP^{316CPM}) were measured in the absence or presence of various concentrations (0.02–0.4 μM) of preEGFP (Fig. 3A–C). The fluorescence intensities of the CPM-labelled MPPs at 465 nm appeared to decrease as the concentration of preEGFP increased, indicating the occurrence of FRET between the CPMs and the EGFP chromophore. Since the FRET efficiency of MPP^{316CPM}/preEGFP was lower than those of the other CPM-labelled MPPs/preEGFP combinations, the acceptor chromophore may be distant from the donor CPM at Cys^{316}. Indeed, it was difficult to calculate the affinity of MPP^{316CPM}/preEGFP via a linear approximation due to the low FRET efficiency. Next, we plotted the decreases in the fluorescence intensities (dF) of MPP^{84CPM} and MPP^{156CPM} against the concentration of preEGFP ([S]), and determined the maximal decreases in the fluorescence intensity (dF_{max}) and the dissociation constants (K_d) using Hanes–Woolf plots (Fig. 3D and E). Furthermore, to determine the quantum yield of the donor (Φ) and overlap integration (J), the absorption spectrum of preEGFP and the fluorescence spectrum were measured. Every measurement was performed three times and the results were averaged. The dissociation constants (K_d) between MPP^{84CPM} or MPP^{156CPM} and preEGFP were calculated to be 93.7 or 112 nM, respectively (Table 1). The similar affinity values obtained for CPM-labelled MPPs/preEGFP suggested that the cysteine substitutions and CPM modifications did not affect the affinity of MPP for the preprotein. Moreover, the K_d values calculated from FRET between MPP and preEGFP were close to those reported by Kojima *et al*. using analyses of a yeast MPP and preMDH peptide substrates (*19*) and similar to the K_m values calculated from kinetic analyses of MPP using presequence peptides as substrates (*16*). Therefore, the CPM modifications little influence substrate binding of MPP and steady state of the enzyme–substrate complex though it is not completely excluded that the chemical modifications effect some steps of over all activity of the enzyme, for example, releasing a presequence peptide from a cavity of MPP. The various parameters required for determining the distance between CPM and the chromophore of EGFP were summarized (Table 1). The distances between the chromophore of preEGFP and MPP^{84CPM} or MPP^{156CPM} were calculated to be 48 or 50 Å, respectively (Table 1) as described in the section 'Experimental Procedures'.

Plausible Structure of the MPP–preEGFP Complex—In the previous complex structure determination of an MPP–substrate complex (PDB ID: 1HR8) (*20*), the signal peptide of COX IV (^{2}LSLRQSIRFFKPATRTLCSSRYLL^{25}) was used for co-crystallization with MPP, although only residues 7–19 were observed in the electron density map. This implies structural flexibility in N- and C-terminal residues 2–6 (LSLRQ) and 20–25 (SSRYLL), respectively. The C-terminal portion is supposed to form part of the loop region linking the presequence and the mature protein. Considering the FRET results and the structural validity, a plausible model of preEGFP complexed with MPP was constructed. The 13 residues of preCOX IV (^{7}SIRFFKPATRTLC^{19}) were replaced with those of preACON (^{5}RSAIKRPIV RGLA^{17}) according to the sequence alignment shown in Fig. 4A. The EGFP structure was superimposed and oriented toward MPP, such that it satisfied the following three geometrical restrictions: 1) no steric hindrance between MPP and preEGFP; 2) distances between the chromophore and residues β-84 and β-156 of MPP of ~48 and ~50 Å, respectively; and 3) distance between Ala^{17} and Gly^{26} of preEGFP of within ~35 Å such that the missing eight residues (^{18}TVSEFVSK^{25}) reasonably bridged the two residues. As a consequence, it was found that the EGFP core domain should be located at the bottom of MPP as shown in Fig. 4B, with its N-terminus (Gly^{26}) facing toward the C-terminus (Ala^{17}) of the bound peptide. This model implies that residues

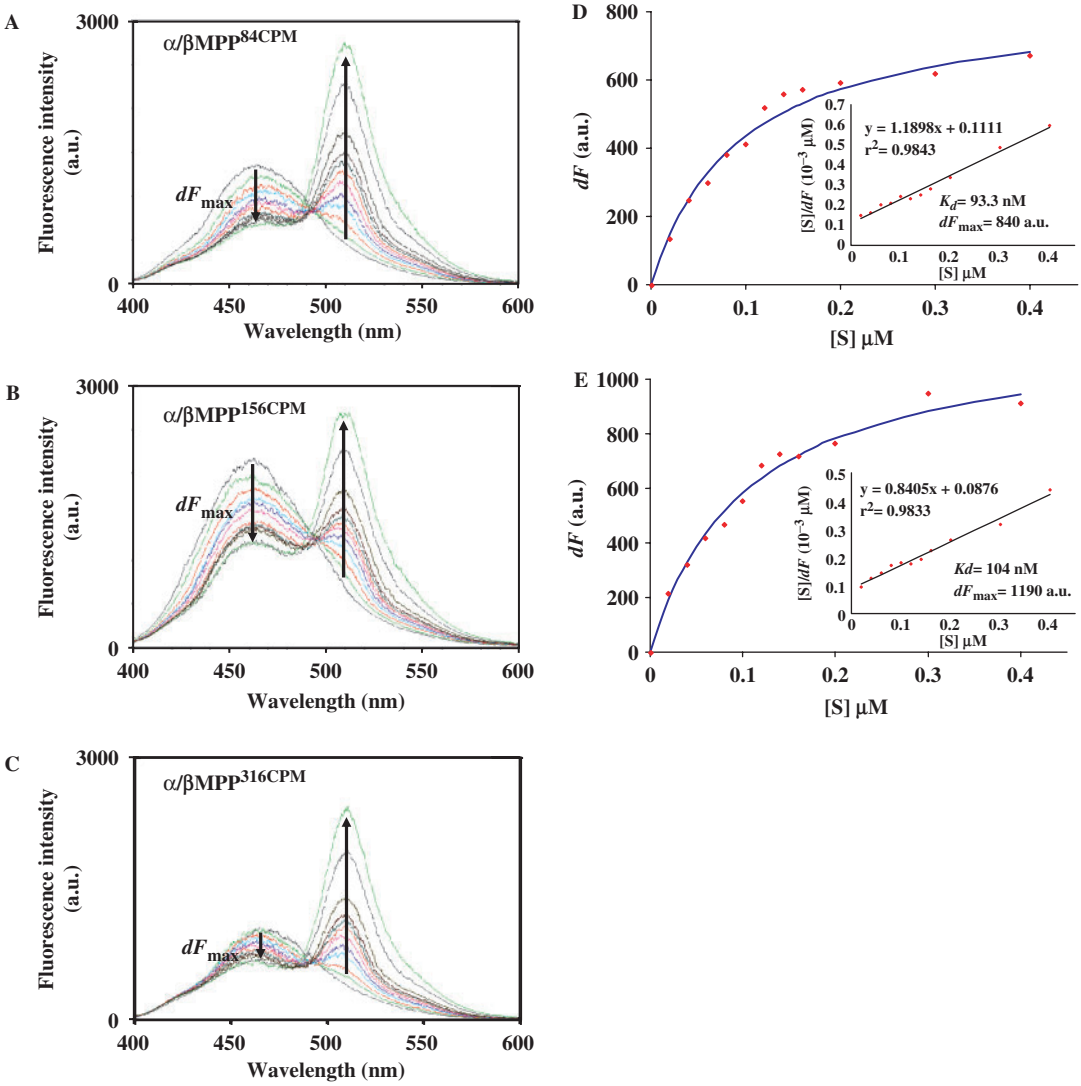

Fig. 3. **FRET measurements and decreases in the fluorescence intensities of CPM-labelled MPPs depend on the concentration of preEGFP.** (A–C) Emission spectra measured as described in the EXPERIMENTAL PROCEDURES. CPM (***A***, α/β-MPP^{84CPM}; ***B***, α/β-MPP^{156CPM} and ***C***, α/β-MPP^{316CPM}) and EGFP have peak fluorescence intensities around 460 and 510 nm, respectively. The arrows suggest that as the concentration of preEGFP increases, the fluorescence intensities of CPM and EGFP decrease or increase, respectively. (D, E) The decreases in the fluorescence intensities (*dF*) of α/β-MPP^{84CPM} (D) and α/β-MPP^{156CPM} (E) were plotted against the concentration of preEGFP ([S]). *Insets*, Hanes–Woolf plots ([S]/*dF* versus [S]). Due to the low FRET efficiency, *dF* versus [S] plots for MPP^{156CPM} were non-saturable and a Hanes–Woolf plot was therefore inappropriate for a linear approximation. All experiments were conducted three times, and representative data are presented. The average values of K_d and dF_{max} were calculated from three individual experiments and are presented in Table 1. a.u., arbitrary units.

18–25 link the signal presequence and the core domain of EGFP in an extended conformation (Fig. 4B and C). Interestingly, the glycine-rich loop of α-MPP (from Gly^{284} to Gly^{297}, Fig. 4B) protrudes toward β-MPP in the middle of the intermolecular cleft and is close to the linking potion of preEGFP. In the previous structure determination, the B-factors of this loop region were considerably high, regardless of the substrate binding (*20*), implying its intrinsic flexibility. The present structure suggests that the C-terminal polypeptide of the signal sequence should stick out through a region in the vicinity of this loop from an acidic cavity composed of both the MPP subunits (Fig. 4C).

DISCUSSION

Our present combinational investigation involving FRET analysis and structural modelling based on the crystal structure of MPP bound to a synthetic peptide has revealed a possible complex orientation of the preprotein toward MPP. Since the physiological substrates of MPP are mitochondrial preproteins rather than peptides, this complex model appears to be implicated in the biological mechanism of preprotein processing in mitochondria.

Here, we again emphasize the significance of the glycine-rich loop of MPP in preprotein processing.

Table 1. **Parameters for determining the distances between the acceptor and donor.**

CPM-MPPs	Φ_D	J ($\times 10^{-13}\,M^{-1}\,cm^3$)	R_0 (Å)	K_d (nM)[a]	E_T[a]	R (Å)[a]
α/β-MPP^{84CPM}	0.960	1.52	53.1	93.7 ± 0.24	0.647 ± 0.028	48.0 ± 1.00
α/β-MPP^{156CPM}	0.907	1.39	51.7	112 ± 7.31	0.550 ± 0.024	50.0 ± 0.81

[a]Mean ± standard deviation (SD), $n = 3$.

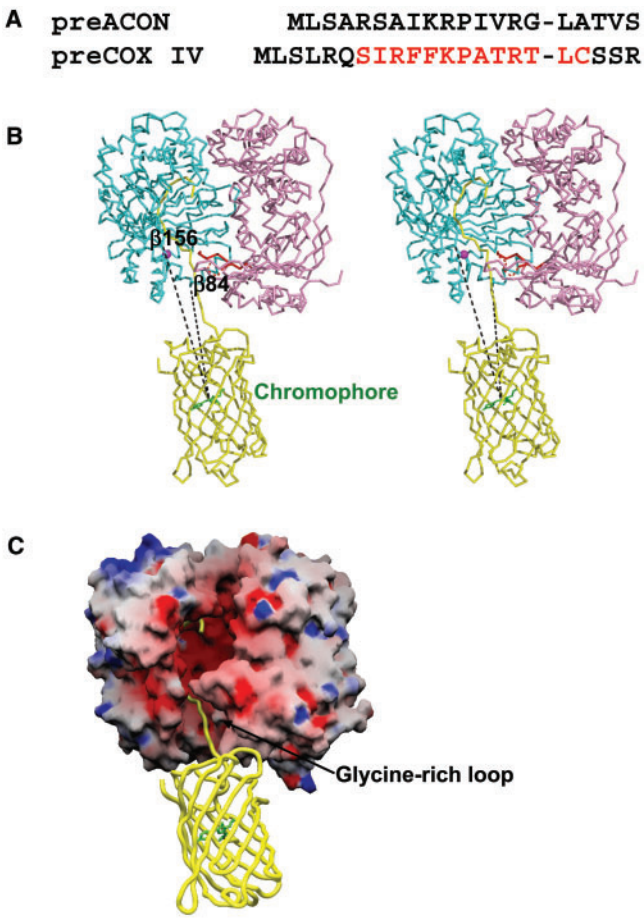

Fig. 4. **Structural model of the MPP/preEGFP complex.** (A) Comparison of the N-terminal amino acid sequences of the yeast preACON and preCOX IV peptides. The preCOX IV residues observed in the electron density map of a crystal structure of the MPP-preCOX IV peptide complex (*20*) are shown in red. Hyphens indicate the cleavage sites of MPP. (B) Stereogram of the plausible complex model. The lilac and cyan tubes display α-MPP and β-MPP, respectively. The structure of preEGFP is displayed as a yellow tube and the chromophore is displayed as a thick green stick. The distances between the chromophore and residues 84 and 156 of β-MPP have been adjusted to ~48 and ~50 Å, respectively. The glycine-rich loop of α-MPP (residues 284–297) is shown in red, and partially disordered (dashed line) in the crystal structure complexed with a peptide (PDB ID: 1HR8). (C) Electrostatic molecular surface representation of yeast MPP complexed with preEGFP. The surface of MPP was calculated using GRASP (*28*) and coloured in the range <-15 to $>+15$ k_BT, where k_B is the Boltzmann constant and T is the temperature. In the MPP structure, the positive potential is shown in blue and the negative potential in red. The glycine-rich loop region is indicated by an arrow. The preEGFP is displayed as a yellow tube with the chromophore displayed as a green stick.

The glycine-rich loop was previously shown to play an essential role in the cleavage of presequences (*26*) and to protrude toward an active site of β-MPP in the middle of the intermolecular cleft (*20*, *26*). Taken together with our MPP–preEGFP structural model, the glycine-rich loop probably interacts with hydrophilic residues linking the presequence and the mature polypeptide, probably with the hydroxyl group of P'_2 and/or P'_3 (Fig. 4B). This interaction could play a role in recognizing the cleavage site and assisting the presequences to interact with the scaffold of MPP in the conformation.

On the other hand, the N-terminal domain of β-MPP presumably interacts with the loop to restrict the flexible conformation. Previous mutational analyses of MPP revealed that Glu^{79} of rat β-MPP, which is equivalent to Glu^{93} of yeast β-MPP, participated in substrate binding and catalysis (*27*), although there was no interaction between Glu^{93} of β-MPP and the COX IV prepeptide in the crystal structure. Glu^{93} of β-MPP is actually close to the main chain amide nitrogens of Gly^{297} and Met^{298} in the glycine-rich loop of α-MPP. Both the main chain nitrogens could be fixed at a regular coordinate by hydrogen bonding with Glu^{93}. Hence, Glu^{93} is not a counterpart of basic amino acid residues in the presequence, but rather plays a role as a factor in turning the glycine-rich loop toward the active centre of β-MPP. The glycine-rich loop region of α-MPP and a loop-interacting glutamate residue of β-MPP may play roles in positioning and assisting the presequences to interact with the scaffold of MPP in the conformation that is most efficient for the protease processing (*13*).

The recently reported crystal structure of presequence protease (PreP) harbouring a substrate peptide in a large proteolytic chamber is amazing, since the single PreP polypeptide responsible for degradation of the signal sequence peptide in both mitochondria and chloroplasts is very similar to the heterodimeric MPP complex in the higher-order structures (*27*). Of more general interest is the action of these peptidases which have large chambers, since a novel mechanism for PreP proteolysis has been proposed involving a hinge-bending motion that causes the protease to open and close the cleft in response to substrate binding. Such a substrate-induced motion of MPP was not observed in the crystal structure with or without a prepeptide. Moreover, the FRET efficiencies between two regiospecific sites in the α-MPP and β-MPP subunits were not affected by the presence or absence of the bound prepeptide in the steady-state (Nishino *et al.*, unpublished results), suggesting little dynamic motion between the subunits. Since PreP has no glycine-rich loop, the MPP action seems to differ from the open and close model of PreP. Further experimental approaches are therefore required to determine the substrate binding and release of MPP in addition to the precise functions of the unique glycine-rich loop.

This work was supported in part by Grants-in-Aid for Scientific Research from the Ministry of Education, Science, Sports and Culture of Japan (No. 12780456 to S.K.) and the Takeda Science Foundation in Japan (to S.K.).

REFERENCES

1. Schechter, I. and Berger, A. (1967) On the size of the active site in proteases. I. Papain. *Biochem. Biophys. Res. Commun.* **27**, 157–162
2. Neupert, W. (1997) Protein import into mitochondria. *Annu. Rev. Biochem.* **66**, 863–917
3. Pfanner, N. and Meijer, M. (1997) The Tom and Tim machine. *Curr. Biol.* **7**, R100–103
4. Endo, T., Yamamoto, H., and Esaki, M. (2003) Functional cooperation and separation of translocators in protein import into mitochondria, the double-membrane bounded organelles. *J. Cell Sci.* **116**, 3259–3267
5. Ito, A. (1999) Mitochondrial processing peptidase: multiple-site recognition of precursor proteins. *Biochem. Biophys. Res. Commun.* **265**, 611–616
6. Oshima, T., Yamasaki, E., Ogishima, T., Kadowaki, K., Ito, A., and Kitada, S. (2005) Recognition and processing of a nuclear-encoded polyprotein precursor by mitochondrial processing peptidase. *Biochem. J.* **385**, 755–761
7. Luciano, P., Tokatlidis, K., Chambre, I., Germanique, J.C., and Geli, V. (1998) The mitochondrial processing peptidase behaves as a zinc-metallopeptidase. *J. Mol. Biol.* **280**, 193–199
8. Luciano, P., Geoffroy, S., Brandt, A., Hernandez, J.F., and Geli, V. (1997) Functional cooperation of the mitochondrial processing peptidase subunits. *J. Mol. Biol.* **272**, 213–225
9. Song, M.C., Shimokata, K., Kitada, S., Ogishima, T., and Ito, A. (1996) Role of basic amino acids in the cleavage of synthetic peptide substrates by mitochondrial processing peptidase. *J. Biochem. (Tokyo)* **120**, 1163–1166
10. Niidome, T., Kitada, S., Shimokata, K., Ogishima, T., and Ito, A. (1994) Arginine residues in the extension peptide are required for cleavage of a precursor by mitochondrial processing peptidase. Demonstration using synthetic peptide as a substrate. *J. Biol. Chem.* **269**, 24719–24722
11. Ogishima, T., Niidome, T., Shimokata, K., Kitada, S., and Ito, A. (1995) Analysis of elements in the substrate required for processing by mitochondrial processing peptidase. *J. Biol. Chem.* **270**, 30322–30326
12. Shimokata, K., Nishio, T., Song, M.C., Kitada, S., Ogishima, T., and Ito, A. (1997) Substrate recognition by mitochondrial processing peptidase toward the malate dehydrogenase precursor. *J. Biochem. (Tokyo)* **122**, 1019–1023
13. Kitada, S., Yamasaki, E., Kojima, K., and Ito, A. (2003) Determination of the cleavage site of the presequence by mitochondrial processing peptidase on the substrate binding scaffold and the multiple subsites inside a molecular cavity. *J. Biol. Chem.* **278**, 1879–1885
14. Shimokata, K., Kitada, S., Ogishima, T., and Ito, A. (1998) Role of alpha-subunit of mitochondrial processing peptidase in substrate recognition. *J. Biol. Chem.* **273**, 25158–25163
15. Kitada, S. and Ito, A. (2001) Electrostatic recognition of matrix targeting signal by mitochondrial processing peptidase. *J. Biochem. (Tokyo)* **129**, 155–161
16. Kitada, S., Kojima, K., and Ito, A. (2001) Glu(191) and Asp(195) in rat mitochondrial processing peptidase beta subunit are involved in effective cleavage of precursor protein through interaction with the proximal arginine. *Biochem. Biophys. Res. Commun.* **287**, 594–599
17. Kojima, K., Kitada, S., Shimokata, K., Ogishima, T., and Ito, A. (1998) Cooperative formation of a substrate binding pocket by alpha- and beta-subunits of mitochondrial processing peptidase. *J. Biol. Chem.* **273**, 32542–32546
18. Abe, Y., Shodai, T., Muto, T., Mihara, K., Torii, H., Nishikawa, S., Endo, T., and Kohda, D. (2000) Structural basis of presequence recognition by the mitochondrial protein import receptor Tom20. *Cell* **100**, 551–560
19. Kojima, K., Kitada, S., Ogishima, T., and Ito, A. (2001) A proposed common structure of substrates bound to mitochondrial processing peptidase. *J. Biol. Chem.* **276**, 2115–2121
20. Taylor, A.B., Smith, B.S., Kitada, S., Kojima, K., Miyaura, H., Otwinowski, Z., Ito, A., and Deisenhofer, J. (2001) Crystal structures of mitochondrial processing peptidase reveal the mode for specific cleavage of import signal sequences. *Structure (Camb)* **9**, 615–625
21. Patterson, G.H., Knobel, S.M., Sharif, W.D., Kain, S.R., and Piston, D.W. (1997) Use of the green fluorescent protein and its mutants in quantitative fluorescence microscopy. *Biophys. J.* **73**, 2782–2790
22. Hanson, G.T., McAnaney, T.B., Park, E.S., Rendell, M.E., Yarbrough, D.K., Chu, S., Xi, L., Boxer, S.G., Montrose, M.H., and Remington, S.J. (2002) Green fluorescent protein variants as ratiometric dual emission pH sensors. 1. Structural characterization and preliminary application. *Biochemistry* **41**, 15477–15488
23. Jones, T.A., Zou, J.Y., Cowan, S.W., and Kjeldgaard., (1991) Improved methods for building protein models in electron density maps and the location of errors in these models. *Acta Crystallogr.* **A 47(Pt 2)**, 110–119
24. Brunger, A.T., Adams, P.D., Clore, G.M., DeLano, W.L., Gros, P., Grosse-Kunstleve, R. W., Jiang, J.S., Kuszewski, J., Nilges, M., Pannu, N.S., Read, R.J., Rice, L.M., Simonson, T., and Warren, G.L. (1998) Crystallography & NMR system: a new software suite for macromolecular structure determination. *Acta Crystallogr. D Biol. Crystallogr.* **54(Pt 5)**, 905–921
25. Collaborative Computational Project, N. (1994) The CCP4 suite: programs for protein crystallography. *Acta Crystallogr. D Biol. Crystallogr.* **50**, 760–763
26. Nagao, Y., Kitada, S., Kojima, K., Toh, H., Kuhara, S., Ogishima, T., and Ito, A. (2000) Glycine-rich region of mitochondrial processing peptidase alpha-subunit is essential for binding and cleavage of the precursor proteins. *J. Biol. Chem.* **275**, 34552–34556
27. Kitada, S., Kojima, K., Shimokata, K., Ogishima, T., and Ito, A. (1998) Glutamate residues required for substrate binding and cleavage activity in mitochondrial processing peptidase. *J. Biol. Chem.* **273**, 32547–32553
28. Nicholls, A., Sharp, K.A., and Honig, B. (1991) Protein folding and association: insights from the interfacial and thermodynamic properties of hydrocarbons. *Proteins* **11**, 281–296